EVLA Memo 219
Enabling MeerKAT Polarimetric Imaging in AIPS

Rick Perley (NRAO), Eric Greisen (NRAO), and Ben Hugo (SARAO)

September 9, 2022

Abstract

We describe the process of calibration and imaging of data taken with a linearly polarized array, with specific examples using MeerKAT data taken at UHF, L, and S0 bands.

1 Introduction and Motivation

In EVLA Memo #207 (2019), Perley and Greisen described their efforts to enable calibration in AIPS of data taken with linearly polarized systems. Before that time, AIPS could only calibrate data from circularly polarized systems, as it was designed specifically for the VLA and VLBA, both of which were engineered to produce circularly polarized data. When the VLA's original circularly-polarized, P-band system, spanning 300 to 340 MHz, was replaced with the new wideband system spanning 230 to 480 MHz, the existing polarizers could not be used, so the data products reverted to the native (linear) system.

Memo #207 was not quite complete – the issue of handling the cross-hand phases was not fully explored. The issue of determining these phases is a significant complication, which deserves a closer treatment, utilizing real data. This is not easily done with the VLA's P-band receivers, as there are no strong linearly polarized calibrators at its low frequency of operation with which to explore the issues.

Since the time Memo #207 was completed, the MeerKAT array has come on line – providing us with data from a well-engineered, linearly polarized system at frequencies (544 – 3500 MHz) where we can observe strongly linearly polarized calibrators. This has enabled us to more thoroughly review and extend the calibration regimen for linearly polarized systems.

2 General Response of an Interferometer

EVLA memo #207 developed the relations between the Stokes' visibilities and the interferometer outputs using a Jones' matrix analysis. For this, the receiver system is considered as a chain for 4-port networks, which traces the path of the voltage signals induced by the electric vector of the incoming radiation from the antenna through to the correlator. This provides a very general and powerful analysis tool, which has been utilized by many authors.

Here we take a different approach, and begin with the remarkable expression[1] presented by Morris, Radhakrishan and Seielstad (Ap.J. **139**, 551) which gives the complex output R_{mn} of a correlation interferometer as a function of the source visibilities[2] $\mathcal{I}, \mathcal{Q}, \mathcal{U}$, and $\mathcal{V}$, and the component antennas' polarization properties Ψ and χ. The relation is[3]:

$$\begin{aligned} R_{mn} \quad = \quad & G_{mn}\{[\cos(\Psi_m - \Psi_n)\cos(\chi_m - \chi_n) + i\sin(\Psi_m - \Psi_n)\sin(\chi_m + \chi_n)]\mathcal{I}/2 \\ & -[\cos(\Psi_m - \Psi_n)\sin(\chi_m + \chi_n) + i\sin(\Psi_m - \Psi_n)\cos(\chi_m - \chi_n)]\mathcal{V}/2 \\ & +[\cos(\Psi_m + \Psi_n)\cos(\chi_m + \chi_n) + i\sin(\Psi_m + \Psi_n)\sin(\chi_m - \chi_n)]\mathcal{Q}/2 \\ & -[\cos(\Psi_m + \Psi_n)\sin(\chi_m - \chi_n) + i\sin(\Psi_m + \Psi_n)\cos(\chi_m + \chi_n)]i\mathcal{U}/2\} \end{aligned} \tag{1}$$

[1] Remarkable because the authors do not derive the expression, nor cite any publication where the derivation is given.

[2] The sign of $\mathcal{V}$ has been negated, in accordance with the IEEE and IAU definitions.

[3] We adopt in this document the formal definition of the Stokes' parameters. However, the major calibration packages (AIPS and CASA, and others) have utilized a definition where the division by two in Eqn 1 is omitted, leading to an overestimation of the gains G_{mn} by a factor of two. This scaling error is removed in the generation of the visibilities from the correlations by dividing by two.

The subscripts m, n denote the nominal polarization state of the two antenna output signals being correlated (i.e., 'h' or 'v'), χ is the antenna polarization ellipticity, Ψ is the position angle, on the sky, of the polarization ellipse major axis, and G_{mn} is the complex system gain for the antenna-polarization pair under consideration. The Stokes visibilities describe the polarization state of the astronomical signal. These visibilities are in general complex valued, although in the case of an unresolved source located at the field phase tracking center, they are real.

Equation (1) is a completely general expression – no approximations are made concerning the purity of the antenna polarization or on the fractional amplitude of the source polarization, nor is any 'basis function' assumed. The expression can be applied to circularly and linearly polarized antennas as well as to all the elliptical states in between.

After some algebraic manipulation, equation (1) can be recast into an alternate form:

$$\begin{aligned} R_{mn} \;=\; & G_{mn}\{[\cos(\chi_m - \chi_n) - \sin(\chi_m + \chi_n)]e^{-i\Delta\Psi}(\mathcal{I} + \mathcal{V})/4 \\ & +[\cos(\chi_m + \chi_n) - \sin(\chi_m - \chi_n)]e^{-i\Sigma\Psi}(\mathcal{Q} + i\mathcal{U})/4 \\ & +[\cos(\chi_m + \chi_n) + \sin(\chi_m - \chi_n)]e^{i\Sigma\Psi}(\mathcal{Q} - i\mathcal{U})/4 \\ & +[\cos(\chi_m - \chi_n) + \sin(\chi_m + \chi_n)]e^{i\Delta\Psi}(\mathcal{I} - \mathcal{V})/4\} \end{aligned} \tag{2}$$

where $\Delta\Psi = \Psi_m - \Psi_n$ is the difference, and $\Sigma\Psi = \Psi_m + \Psi_n$ is the sum, of the two polarization ellipse position angles for the polarization pair under consideration. The advantage of this form is that two key dependencies are now clearly shown: the antenna polarization ellipse position angles affect only the phase of the observed visibilities, while the antenna polarization ellipticities affect only the amplitudes of the observed visibilites.

The polarization ellipticity χ is defined as the arctangent of the ratio of the minor to major axes of the antenna polarization ellipse. The amplitude of this ratio varies from zero for purely linearly polarized antennas, to unity for purely circularly polarized antennas. By convention, χ is negative for right elliptically polarized radiation, and positive for left elliptically polarized radiation. Hence, $|\chi|$ varies from 0 for linear to $\pi/4$ for circularly polarized antennas.

As this memo deals with polarimetry using well-designed linearly-polarized receivers, we will now make the approximation that the purity of the linearly polarized feeds is very good – which in the terms of the definitions above, means the ellipticity is very low: $|\chi| \ll 1$.

2.1 Pure Linearly Polarized Antennas

We start by generating the interferometer responses for a pure linearly polarized system, for which $\chi = 0$. For simplicity, assume now that the antenna feeds are orthogonal and correctly oriented so that the 'V' feed is vertical. Equation 1 then simplifies to

$$2R_{mn}/G_{mn} = \mathcal{I}\cos(\Psi_m - \Psi_n) - i\mathcal{V}\sin(\Psi_m - \Psi_n) + \mathcal{Q}\cos(\Psi_m + \Psi_n) + \mathcal{U}\sin(\Psi_m + \Psi_n) \tag{3}$$

Results for the four separate correlations are then derived by setting the vertical feed position angle to the parallactic angle[4] Ψ_p and the horizontal feed to $\pi/2 + \Psi_p$, since we are assuming the antennas are 'Az-El' mounted. We find:

$$2R_{vv}/G_{vv} = \mathcal{I} + \mathcal{Q}\cos 2\Psi_p + \mathcal{U}\sin 2\Psi_p \tag{4}$$
$$2R_{vh}/G_{vh} = -\mathcal{Q}\sin 2\Psi_p + \mathcal{U}\cos 2\Psi_p + i\mathcal{V} \tag{5}$$
$$2R_{hv}/G_{hv} = -\mathcal{Q}\sin 2\Psi_p + \mathcal{U}\cos 2\Psi_p - i\mathcal{V} \tag{6}$$
$$2R_{hh}/G_{hh} = \mathcal{I} - \mathcal{Q}\cos 2\Psi_p - \mathcal{U}\sin 2\Psi_p \tag{7}$$

where we have replaced the generic 'm' and 'n' labels with 'v' (for vertical) and 'h' (for horizontal)[5].

The visibilities are then given by

$$\mathcal{I} = R'_{vv} + R'_{hh} \tag{8}$$
$$i\mathcal{V} = R'_{vh} - R'_{hv} \tag{9}$$
$$\mathcal{Q} = (R'_{vv} - R'_{hh})\cos 2\Psi_p - (R'_{vh} + R'_{hv})\sin 2\Psi_p \tag{10}$$
$$\mathcal{U} = (R'_{vv} - R'_{hh})\sin 2\Psi_p + (R'_{vh} + R'_{hv})\cos 2\Psi_p \tag{11}$$

[4] $\Psi_p = \frac{\sin H}{\cos\delta\tan\phi - \sin\delta\cos H}$, where ϕ is the antenna's latitude.

[5] Discussion of the important issue of the phase offset between the 'V' and 'H' channels is deferred to Section 4.7, in order to simplify the presentation. For this section, we presume that all such phases are included in the complex gains G_{mn}.

where the primed symbols indicates the gain calibration factors G_{mn} have been applied.

Note that all four correlations are in general required to derive the $\mathcal{Q}$ and $\mathcal{U}$ Stokes visibilities – a contrast with circularly polarized systems, where only the cross-hand visibilities are required. The need to subtract the generally large amplitude parallel-hand visibilities for the determination of the linear polarization is generally considered a negative feature of linearly polarized systems, as a higher level of stability and calibration is required to obtain accurate results. On the other hand, the Stokes V visibility is derived from the difference between the (usually small) cross-correlations – generally considered an advantage. For circularly polarized systems, the situation is reversed – the Stokes 'V' visibility is formed from the difference of the parallel-hand channels, while the linearly polarized parameters are formed from the cross-hand visibilities alone.

2.2 Nearly Perfect Linear

For nearly perfectly linear systems, $\chi \ll 1$. We now follow the analysis of Thompson, Moran, and Swenson (TMS) and set the cosine factors involving the χ terms to unity, and replace the sine factors by their first-order expansions. The fundamental relation (eqn 1) becomes

$$\begin{aligned} 2R_{mn}/G_{mn} &= \mathcal{I}(\cos\Delta\Psi_{mn} + i\Sigma\chi_{mn}\sin\Delta\Psi_{mn}) - i\mathcal{V}(\sin\Delta\Psi_{mn} - i\Sigma\chi_{mn}\cos\Delta\Psi_{mn}) \\ &\quad + \mathcal{Q}(\cos\Sigma\Psi_{mn} + i\Delta\chi_{mn}\sin\Sigma\Psi_{mn}) + \mathcal{U}(\sin\Sigma\Psi_{mn} - i\Delta\chi_{mn}\cos\Sigma\Psi_{mn}) \end{aligned} \tag{12}$$

where $\Sigma\Psi_{mn}$ and $\Delta\Psi_{mn}$ are the sums and differences of the antenna polarization ellipse position angles for the polarization pair under consideration, and $\Sigma\chi_{mn}$ and $\Delta\chi_{mn}$ are the sums and differences of the antenna polarization ellipticities for the antenna polarization pair under consideration.

For notational simplicity, we now assume that all antennas have the same parallactic angle Ψ_p. Relaxing the restriction is straighforward, but introduces algebraic complexity, which we wish to avoid. We then introduce θ_v and θ_h as the misorientations of the nominally vertical and horizontal feeds with respect to the true vertical and horizontal. Expressions for the four correlations can then be determined by specifying $\Psi_v = \Psi_p + \theta_v$, and $\Psi_h = \Psi_p + \pi/2 + \theta_h$. As an example, for the 'VV' correlation, we get $\Delta\Psi_{vv} = \theta_{v1} - \theta_{v2} = \Delta\theta_{vv}$, and $\Sigma\Psi_{vv} = 2\Psi_p + \theta_{v1} + \theta_{v2} = 2\Psi_p + \Sigma\theta_{vv}$, leading to

$$\begin{aligned} 2R_{vv}/G_{vv} &= \mathcal{I}[\cos\Delta\theta_{vv} + i\Sigma\chi_{vv}\sin\Delta\theta_{vv}] - i\mathcal{V}[\sin\Delta\theta_{vv} - i\Sigma\chi_{vv}\cos\Delta\theta_{vv}] \\ &+ \mathcal{Q}[\cos(2\Psi_p + \Sigma\theta_{vv}) + i\Delta\chi_{vv}\sin(2\Psi_p + \Sigma\theta_{vv})] + \mathcal{U}[\sin(2\Psi_p + \Sigma\theta_{vv}) - i\Delta\chi_{vv}\cos(2\Psi_p + \Sigma\theta_{vv})] \end{aligned} \tag{13}$$

with similar expressions for the other three correlations.

We now introduce the last small-angle approximation – that the feed misorientation angles $\theta_v, \theta_h \ll 1$. We define the leakage ('D') term[6] as $D = \theta - i\chi$, so that:

$$D_v = \theta_v - i\chi_v \tag{14}$$
$$D_h = \theta_h - i\chi_h \tag{15}$$

Note that the effects of feed misorientations are manifest in the real part of these terms, and those of polarization ellipticity in the imaginary part.

We then arrive at our equation set for nearly-pure linearly-polarized systems:

$$\begin{aligned} 2R_{vv}/G_{vv} &= \mathcal{I} - i\mathcal{V}(D_{v1} - D^*_{v2}) \\ &\quad + \mathcal{Q}[\cos 2\Psi_p - (D_{v1} + D^*_{v2})\sin 2\Psi_p] + \mathcal{U}[\sin 2\Psi_p + (D_{v1} + D^*_{v2})\cos 2\Psi_p] \end{aligned} \tag{16}$$
$$\begin{aligned} 2R_{vh}/G_{vh} &= \mathcal{I}[D_{v1} - D^*_{h2}] + i\mathcal{V} \\ &\quad - \mathcal{Q}[\sin 2\Psi_p + (D_{v1} + D^*_{h2})\cos 2\Psi_p] + \mathcal{U}[\cos 2\Psi_p - (D_{v1} + D^*_{h2})\sin 2\Psi_p] \end{aligned} \tag{17}$$
$$\begin{aligned} 2R_{hv}/G_{hv} &= -\mathcal{I}[D_{h1} - D^*_{v2}] - i\mathcal{V} \\ &\quad - \mathcal{Q}[\sin 2\Psi_p + (D_{h1} + D^*_{v2})\cos 2\Psi_p] + \mathcal{U}[\cos 2\Psi_p - (D_{h1} + D^*_{v2})\sin 2\Psi_p] \end{aligned} \tag{18}$$
$$\begin{aligned} 2R_{hh}/G_{hh} &= \mathcal{I} - i\mathcal{V}(D_{h1} - D^*_{h2}) \\ &\quad - \mathcal{Q}[\cos 2\Psi_p - (D_{h1} + D^*_{h2})\sin 2\Psi_p] - \mathcal{U}[\sin 2\Psi_p + (D_{h1} + D^*_{h2})\cos 2\Psi_p] \end{aligned} \tag{19}$$

[6]Note that our definition of D_h is negated from that of TMS – we choose this form as it improves the form of the resulting equations.

Deriving the formal solutions for the Stokes' visibilities is somewhat tedious – the procedure, which involves matrix methods, will be described in a later memo. The solutions are (presuming the gains are applied)[7]:

$$
\begin{aligned}
\mathcal{I} &= R'_{vv} + R'_{hh} + R'_{vh}(D_{h1} - D^*_{v2}) - R'_{hv}(D_{v1} - D^*_{h2}) && (20)\\
i\mathcal{V} &= R'_{vh} - R'_{hv} - R'_{vv}(D_{h1} - D^*_{h2}) - R'_{hh}(D_{v1} - D^*_{v2}) && (21)\\
\mathcal{Q} &= R'_{vv}[\cos 2\Psi_p - (D_{h1} + D^*_{h2})\sin 2\Psi_p] - R'_{hh}[\cos 2\Psi_p - (D_{v1} + D^*_{v2}]\sin 2\Psi_p] \\
&\quad - R'_{vh}[\sin 2\Psi_p + (D_{h1} + D^*_{v2})\cos 2\Psi_p] - R'_{hv}[\sin 2\Psi_p + (D_{v1} + D^*_{h2})\cos 2\Psi_p] && (22)\\
\mathcal{U} &= R'_{vv}[\sin 2\Psi_p + (D_{h1} + D^*_{h2})\cos 2\Psi_p] - R'_{hh}[\sin 2\Psi_p + (D_{v1} + D^*_{v2}]\cos 2\Psi_p] \\
&\quad + R'_{vh}[\cos 2\Psi_p - (D_{h1} + D^*_{v2})\sin 2\Psi_p] + R'_{hv}[\cos 2\Psi_p - (D_{v1} + D^*_{h2})\sin 2\Psi_p] && (23)
\end{aligned}
$$

In many circumstances, we can assume the Stokes' $\mathcal{Q}$, $\mathcal{U}$, and $\mathcal{V}$ visibility amplitudes are much less than those of $\mathcal{I}$. In such cases, we can dispense with products of these terms with the leakage terms. This gives us the well-known relations

$$
\begin{aligned}
2R_{vv}/G_{vv} &= \mathcal{I} + \mathcal{Q}\cos 2\Psi_p + \mathcal{U}\sin 2\Psi_p && (24)\\
2R_{vh}/G_{vh} &= \mathcal{I}[D_{v1} - D^*_{h2}] - \mathcal{Q}\sin 2\Psi_p + \mathcal{U}\cos 2\Psi_p + i\mathcal{V} && (25)\\
2R_{hv}/G_{hv} &= -\mathcal{I}[D_{h1} - D^*_{v2}] - \mathcal{Q}\sin 2\Psi_p + \mathcal{U}\cos 2\Psi_p - i\mathcal{V} && (26)\\
2R_{hh}/G_{hh} &= \mathcal{I} - \mathcal{Q}\cos 2\Psi_p - \mathcal{U}\sin 2\Psi_p && (27)
\end{aligned}
$$

At the same level of approximation, ignoring products between the cross-hand visibilities and the leakages, we find for the derived Stokes' visibilities:

$$
\begin{aligned}
\mathcal{I} &= R'_{vv} + R'_{hh} && (28)\\
i\mathcal{V} &= R'_{vh} - R'_{hv} - R'_{vv}(D_{h1} - D^*_{h2}) - R'_{hh}(D_{v1} - D^*_{v2}) && (29)\\
\mathcal{Q} &= R'_{vv}[\cos 2\Psi_p - (D_{h1} + D^*_{h2})\sin 2\Psi_p] - R'_{hh}[\cos 2\Psi_p - (D_{v1} + D^*_{v2})\sin 2\Psi_p] \\
&\quad - (R'_{vh} + R'_{hv})\sin 2\Psi_p && (30)\\
\mathcal{U} &= R'_{vv}[\sin 2\Psi_p + (D_{h1} + D^*_{h2})\cos 2\Psi_p] - R'_{hh}[\sin 2\Psi_p + (D_{v1} + D^*_{v2})\cos 2\Psi_p] \\
&\quad + (R'_{vh} + R'_{hv})\cos 2\Psi_p && (31)
\end{aligned}
$$

Note that in the special case of an unpolarized source, the equation set becomes

$$
\begin{aligned}
2R_{vv}/G_{vv} &= \mathcal{I} && (32)\\
2R_{vh}/G_{vh} &= \mathcal{I}[D_{v1} - D^*_{h2}] && (33)\\
2R_{hv}/G_{hv} &= -\mathcal{I}[D_{h1} - D^*_{v2}] && (34)\\
2R_{hh}/G_{hh} &= \mathcal{I} && (35)
\end{aligned}
$$

which is of particular interest for calibration purposes.

3 Symmmetry Properties for I, Q, U, and V

The AIPS software assumes the input data streams adhere to the IAU standard – the four correlations, nominally labelled 'XX', 'YY', 'XY', and 'YX', physically correspond to the 'VV', 'HH', 'VH', and 'HV' correlations, and the phase relation between the vertical and horizontal dipoles will generate a signal from the horizontal dipole which lags that from the vertical dipole by 90 degrees, for an incoming RCP electric field. This is important as the correlation combinations described in the previous section which are used to form the Stokes' visibilities must conform to the standards assumed by the software. If the actual signal identifications do not correspond to the order shown above, curious results will be found, as shown next, using actual MeerKAT observations of the Moon at 867 MHz.

We illustrate this point with two scenarios:

- The axis identifications are reversed. In this case the presumed vertical component is actually the horizontal, and vice versa.

[7]These expressions are not given in TMS, so we cannot guarantee all signs are correct.

- One of the feeds is connected ‘backwards’. In this case the voltages from that feed are negated (phase shifted by 180 degrees) with respect to the assumed standard.

Analysis is simplest if we ignore the effects of rotation due to parallactic angle (inclusion of this does not change the results).

We denote by $\mathcal{E}_v$ and $\mathcal{E}_h$ the analytic fields corresponding to the true vertical and horizontal electric fields. The four Stokes’ parameters are defined as

$$\mathcal{I} = <\mathcal{E}_{v1}\mathcal{E}^*_{v2}> + <\mathcal{E}_{h1}\mathcal{E}^*_{h2}> \quad (36)$$
$$\mathcal{Q} = <\mathcal{E}_{v1}\mathcal{E}^*_{v2}> - <\mathcal{E}_{h1}\mathcal{E}^*_{h2}> \quad (37)$$
$$\mathcal{U} = <\mathcal{E}_{v1}\mathcal{E}^*_{h2}> + <\mathcal{E}_{h1}\mathcal{E}^*_{v2}> \quad (38)$$
$$i\mathcal{V} = <\mathcal{E}_{v1}\mathcal{E}^*_{h2}> - <\mathcal{E}_{h1}\mathcal{E}^*_{v2}> \quad (39)$$

The questions are: What is the effect of an error in labelling, and, what is the effect of negating one of the voltage streams (equivalent to reversal in the feed wiring). The answers are easily deduced from the equation set above, and are summarized in the following table.

Operation	Orientation	Normal	Swapped	Normal	Swapped
	Phasing	Normal	Normal	Negated	Negated
$<\mathcal{E}_{v1}\mathcal{E}^*_{v2}> + <\mathcal{E}_{h1}\mathcal{E}^*_{h2}>$		I	I	I	I
$<\mathcal{E}_{v1}\mathcal{E}^*_{v2}> - <\mathcal{E}_{h1}\mathcal{E}^*_{h2}>$		iV	-iV	-iV	iV
$<\mathcal{E}_{v1}\mathcal{E}^*_{h2}> + <\mathcal{E}_{h1}\mathcal{E}^*_{v2}>$		Q	-Q	Q	-Q
$<\mathcal{E}_{v1}\mathcal{E}^*_{h2}> - <\mathcal{E}_{h1}\mathcal{E}^*_{v2}>$		U	U	-U	-U

The effects on a polarization image due to the mislabelling or incorrect phasing can be quite remarkable. Shown in Fig 1 are the images derived for observations of the Moon, taken with the MeerKAT UHF system at 867 MHz, with the errors (or mislabels) shown in the table above.

The correct polarization result is shown in the upper left panel – the E-fields point radially outwards. If, however, the signals streams are interchanged, the result is as shown in the upper right panel: Q is negated, while U is unaffected. The bottom two panels show the effect of introducing a phase error of 180 degrees between the two feeds. The bottom left shows the result when the orientation definitions are correct: Q is correct, U is negated, and the bottom right shows the result when the definitions are reversed: both Q and U are negated, turning the radial field distribution into a azimuthal field distribution.

In this illustrative example, the cross-hand phase error assumed here is 180 degrees (i.e., as if the feed were wired backwards). This is a restrictive assumption, made here only for pedagogical reasons, as the cross-hand phase can have any value, not just 0 or 180, due to the electronics and any cross-hand delay. The effect of an arbitrary phase difference on the imaging is rather more subtle, and is addressed in Section 4.7.

4 Calibrating MeerKAT Data in AIPS

The genesis of this memo is a project to determine the true electric vector position angle (EVPA) for 3C286 at low frequencies. In a 2013 paper, Perley and Butler (ApJS, **206**, 16) showed that the EVPA for 3C286 rises from the accepted standard of 33 degrees at 8 GHz to approximately 38 degrees at 48 GHz. This was determined by polarmetric imaging of the planet Mars using data taken as part of the long-running VLA calibrator flux density monitoring program. The EVPA of the Martian emission must be perfectly radial, so any observed rotation from radial measured in the Martian images must be due to offsets in the presumed EVPA of 3C286 which was used to calibrate the VLA data.

The PB2013 result applies only to high frequencies, as the calibrator flux density monitoring program data were taken in ‘C’ and ‘D’ configurations, so did not have the spatial resolution to determine any EVPA offsets in 3C286 at frequencies below 8 GHz.

The MeerKAT array is designed for polarimetric imaging at low frequencies. As the receivers produce linear data, the observed EPA for an astronomial object is fixed by the orientation of the antenna dipoles, and does not require an observation of the EPA of an external source. The accuracy of the MeerKAT dipoles is not well determined, and errors of a few degrees are likely. Furthermore (and perhaps most importantly), it is of considerable importance that the VLA and MeerKAT produce the same results for observations within the range of frequency overlap – 980 to

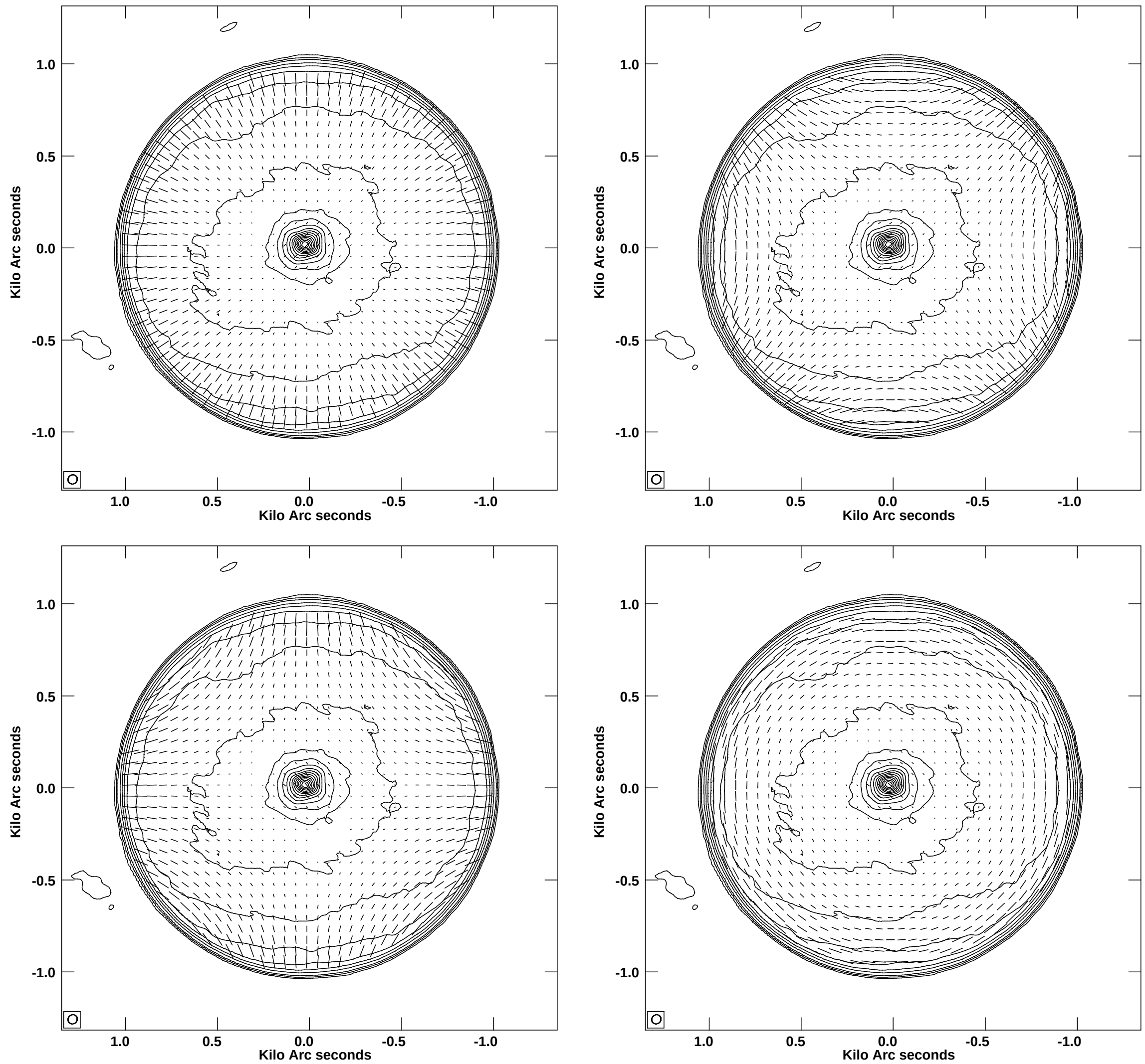

Figure 1: Polarimetric images of the Moon, at 867 MHz, taken with MeerKAT, showing the effects of certain errors in polarimetric imaging. The bright central emission is due to reflected terrestrial RFI. **Upper Left** Correct feed orientation and phasing. The polarization vectors are correctly oriented. **Upper Right** H and V feeds swapped, phasing correct. **Lower Left** Correct feed orientations, one feed connection reversed. **Lower Right** Feed orientations swapped, connection of one feed negated.

3500 MHz. Thus, derivation of the true EPA of polarization standards such as (and most importantly) 3C286 at low frequencies is an important project for both arrays. We point out also that the issue of accurately determining the cross-hand phase requires use of a strong source with accurately known polarization.

To do this, MeerKAT staff has recently employed the same technique to determine the true EVPA of 3C286 at their operating frequencies – ∼550 through 3500 MHz, using the Moon as the EVPA calibrator, since the array does not have the resolution to resolve the Martian emission. Because we wanted to improve our understanding of the calibration of polarimetry data using a linearly polarized system, we obtained copies of the three MeerKAT lunar observations at their UHF, L, and S bands[8] with the goal of utilizing AIPS for the calibration and imaging.

Various difficulties were encountered in our attempts to successfully calibrate these datasets. In particular, with only one or two observations of the highly polarized calibrator 3C286, it proved very difficult to sort out both the feed orientations (which feed is horizontal, which vertical), and to determine the phase relationship between the feeds. To assist in resolving these issues, we requested special four-hour-long continuous observations of the polarized

[8]These observations were taken in June and August, 2021, under Program COM-20210505-BH-01. The schedule blocks are 20210818-0008 at L-band, 20210626-0017 at S0 band, and 20210622-0005 at UHF band.

calibrator 3C286 at all three bands. These observations[9] were taken in June, 2022. The UHF band data spanned 544 to 1088 MHz, the L band data 856 to 1711 MHz, and the S0 band data from 1750 to 2625 MHz. The results shown below are taken from these test observations.

4.1 Spectral Window Structure

AIPS has been designed to work with the EVLA's spectral window structures. The visibility data generated by the WIDAR correlator are organized into 'spectral windows' which for wide-band applications are typically comprised of 16 adjacent spectral blocks, each of 128 MHz width. The MeerKAT correlator does not utilize this concept, and provides the data in a single 'window', covering the entire frequency span.

Although AIPS is capable of managing the data from a single wide block, we have for convenience elected to subdivide the MeerKAT data into the familiar 'WIDAR-like' structure, with 16 adjacent 'spectral windows', using the program 'MORIF'.

4.2 Feed Orientation

The first issue encountered is the orientation of the feeds. The MeerKAT data came to us with labels 'X' and 'Y', but with no information of which is identified with the horizontal feed and which is vertical. By default, AIPS presumes the IAU definitions – the 'X' labelled feed is vertical, the 'Y' labelled feed is horizontal. This turned out to be incorrect – the identifications are reversed. Described below is how we determined this.

The polarization of 3C286 at frequencies above 1 GHz is very well known from VLA observations. At ~ 1 GHz, the fractional linear polarization[10] is $P/I = \sqrt{Q^2 + U^2}/I \sim 0.1$, with a position angle $\Psi_{src} \sim 30$ degrees. With these parameters, defining $Q/I = P\cos 2\Psi_{src}$, $U/I = P\sin 2\Psi_{src}$, and ignoring the small leakage terms, the flux-normalized gain-calibrated correlator responses are[11]:

$$
\begin{aligned}
R'_{vv}/I &= 1 + P\cos 2(\Psi_{src} - \Psi_p) && (40)\\
R'_{vh}/I &= P\sin 2(\Psi_{src} - \Psi_p) && (41)\\
R'_{hv}/I &= P\sin 2(\Psi_{src} - \Psi_p) && (42)\\
R'_{hh}/I &= 1 - P\cos 2(\Psi_{src} - \Psi_p) && (43)
\end{aligned}
$$

This simplified equation set provides an easy way to check the feed labelling assignments. In Fig 2 we show the expected normalized parallel-hand visibilites for 3C286 as observed by MeerKAT, at $\sim$1 GHz, along with actual data from the UHF-band observations. The left panel shows the expected parallel-hand normalized visibilities. The red trace shows the output from correlation of the two vertical feeds, the blue from the two horizontal feeds. The 'VV' output must rise with increasing parallactic angle, while the horizontal feed response 'HH' (blue) will decline. The two are equal at a parallactic angle equal to the source EPA + 135 degrees (and also at $\pm$90 and 180 degrees away from this). The central panel shows the observed visibilities from the nominal 'XX' correlation (red) and 'YY' correlation (blue) for data loaded into AIPS from the 'uvfits' file provided us. From this, it is obvious that the polarization channel assignments are reversed. The right panel shows the data after the AIPS program SWPOL has been applied. The designations are now correct[12].

Repeating this operation for all three MeerKAT datasets revealed that all have their polarization assignments reversed with respect to that assumed by AIPS. The AIPS' 'FITLD' and 'UVLOD' programs have thus been modified to recognize MeerKAT data, and to automatically reverse the polarization identifications.

The problem arises because the MeerKAT visibility format has the data stored as (HH, VV, VH, HV), which upon conversion to uvfits has been identified with (XX, YY, XY, YX)[13].

4.3 Parallel Hand Delay and Phase Calibration

Once the feed orientations are known, we can proceed with regular parallel-hand calibration. The first step is to measure and remove the parallel-hand delays. In AIPS, this is done with the program 'FRING', which solves for both

[9] Program EXT-20220615-BH-01. The SB ids are 20220617-0005 at S0 band, 20220615-0007 at UHF band, and 20220615-0008 at L band.

[10] We here assume for simplicity that the calibrator is a point source, so the Stokes' Q and U values are real

[11] We are here using the AIPS and CASA definitions, to allow comparison to the actual data.

[12] Astute readers will note that the two visibility plots shown in Fig 2 have amplitudes about 2% above those expected. This is due to our selection of a short spacing baseline for this illustration – the added visibility amplitude is due to the background sources in the field.

[13] This applies also to Measurement Set converted data.

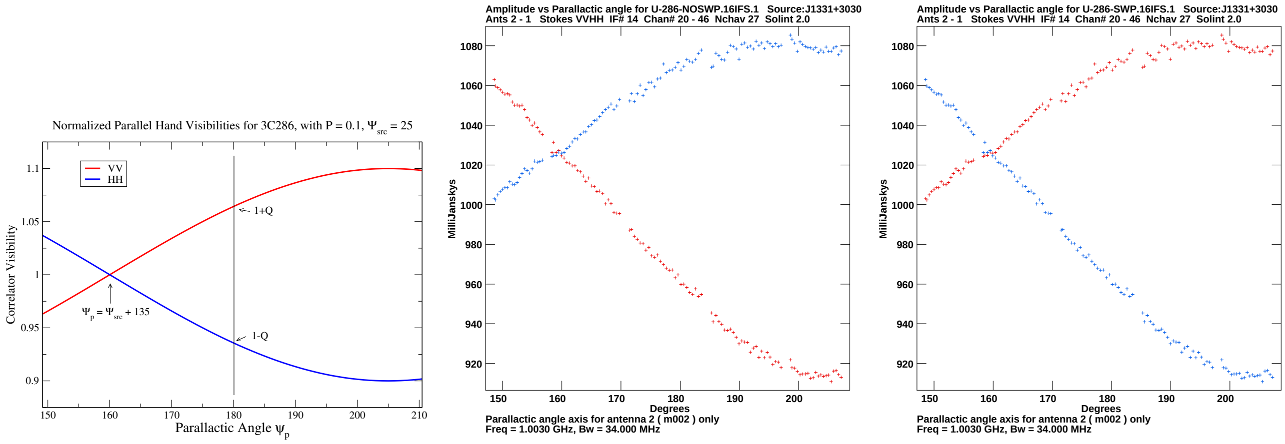

Figure 2: **Left Panel** The expected parallel-hand normalized visibilities for 3C286 at 1 GHz, for the parallactic range visible to MeerKAT. **Central Panel** The observed visibilities, assuming the 'X' axis is vertical – The identification of the vertical and horizontal feeds is incorrect. **Right Panel** The visibilities after swapping the identifications. The assignments are correct.

the delays and phases with respect to a chosen reference antenna – we selected m002 for this. A slight dependence of the phase solutions on the polarization state of the calibrator is possible, as the Q and U emission may not be spatially aligned with that of I. This will be small in any event, and we have elected to ignore this at present.

The phase stability for all observations was very good. We show in Fig 3 typical phase solutions for 'V' and 'H', and the (V-H) phase differences, for three antennas – m000, m025, and m058 in the UHF data. These were chosen to represent a short, intermediate, and long spacing with respect to the reference antenna, m002. Solutions from J1939-6342 are in blue, 3C286 in red. The significant phase offset seen between the solutions for these two

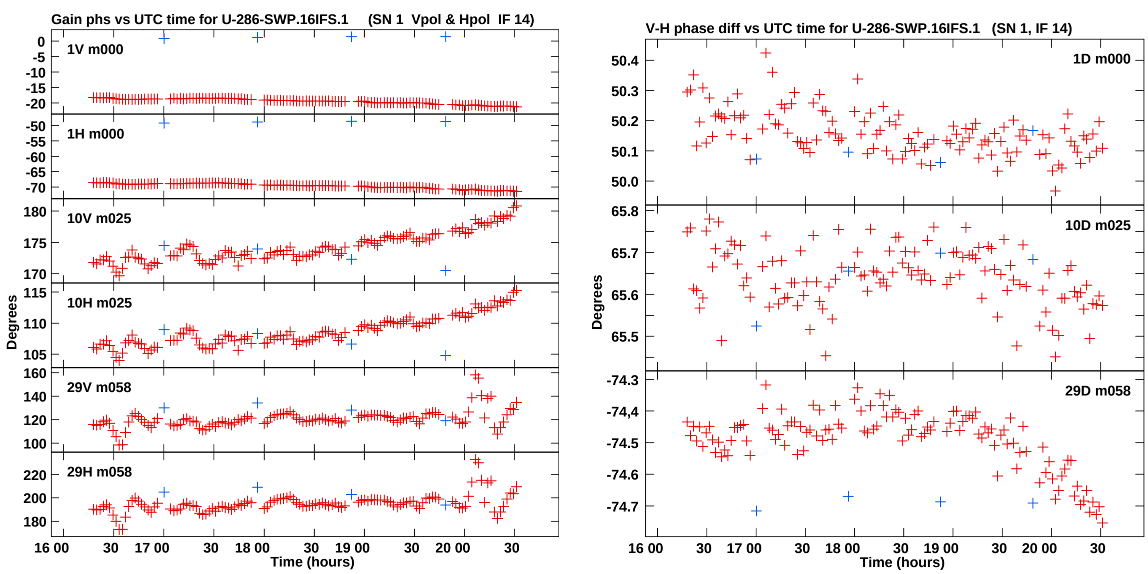

Figure 3: MeerKAT phase solutions at 1.0 GHz, from the UHF data. Red points are from 3C286, blue points from the unpolarized flux calibrator J1939-6342. **Left Panel** The observed phase solutions, for both 'V' and 'H' channels, for a short, intermediate, and long baseline. **Right Panel** The 'V-H' phase differences for the same antennas. The reference antenna, m002, is located near the center of the array.

calibrators for antenna m000 is due to an error in the position of that antenna, which must be almost entirely in the 'z' coordinate (parallel to the earth's axis of rotation) as it is nearly constant over the duration of the observation, or in the axis offset term 'k'. This offset is not seen in the more distant antennas, but is present in most of the central ones.

Notable characteristics in these plots are the excellent phase stability (keeping in mind that the elevation of 3C286 in these observations is between 23 and 29 degrees), and the very small scatter in the phase differentials between the parallel hands – typically less than ~ 0.1 degrees. The phase differentials themselves can be very large – this has significant observational consequences, which are discussed in Section 4.7.

4.4 Bandpass Calibration

The next step is to remove the frequency-dependent gains caused by the electronics. This is done by the program BPASS, which finds the amplitudes and phases (w.r.t. the reference antenna) for each spectral channel across the entire bandpass. We again took m002 as the reference.

This is the first place where we meet the problem of polarized calibrators. Because the parallel-hand visibilities for a linearly-polarized system are sensitive to the source linear polarization, as shown in equations 4 and 7, we need to know the source polarization in order to prevent the polarization being absorbed into the gains[14]. Gain calibration is most easily done if the calibrator is known to be unpolarized. We utilized the standard southern flux density calibrator J1939 − 6342, which is known to be unpolarized to a very low level. In general, if using a linearly-polarized calibrator for determination of the bandpass, the source polarization needs to be known in advance.

Shown in Fig 4 are the resulting 'absolute' bandpasses for four antennas. The bandpasses are quite smooth with

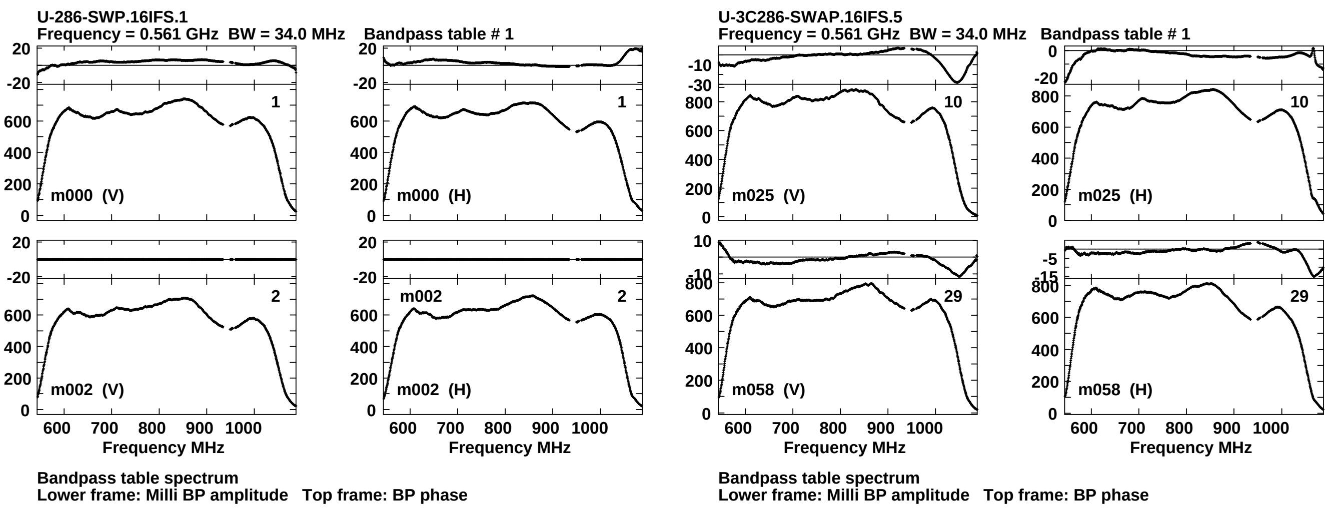

Figure 4: Absolute bandpass solutions for four MeerKAT antennas at UHF band. Each plot shows the phase on top, and the amplitude below. Antenna m002 is the phase reference. **Left Panel** Antennas m000 and m002. **Right Panel** Solutions for m025 and m058. The solutions show very little frequency structure other than the rolloffs at the ends caused by the analog passband filters following the receiver LNA. Gaps are due to RFI blanking.

small undulations, except at the edges.

One can avoid the need for knowledge of the source polarization for this step by utilizing bandpass normalization – the average bandpass gain is scaled to 1.0, separately for each polarization. This removes the bandpass shapes, but leaves in any average gain difference, which must be removed by the subsequent amplitude calibration. There is no functional advantage to this approach unless the bandpass calibrator has unknown polarization, and there are no other suitable sources for determining the bandpass shapes.

4.5 Gain Amplitude Calibration

With the bandpasses determined, we move on to the amplitude calibration. Here again, correct solutions can only be found if the polarization of the calibrator source is known – or can be derived from the data in hand[15]. Since the fractional polarization and EVPA of 3C286 are known, this information has been utilized in the determination of the parallel-hand gains in. AIPS now utilizes the values of 'Q' and 'U' found in the SU table[16]. In Fig 5 we show the

[14]Using these gains would result in the disappearance of the source polarization in subsequent imaging!

[15]In principle, the polarization state of the calibrators can be derived from data taken over a sufficiently wide range in parallactic angle, as is regularly done with the circularly-polarized VLA antennas. AIPS does not yet have this capability for linearly polarized systems.

[16]But only as a point-source. Software to utilize complete models in I, Q, and U has been written, but not yet tested.

gain solutions from the unpolarized calibrator J1939-6342 (in blue), and the highly polarized calibrator J1331+3030 = 3C286 (in red). In this figure the individual 'V' and 'H' gains are shown in the left panel, the ratio of these gains

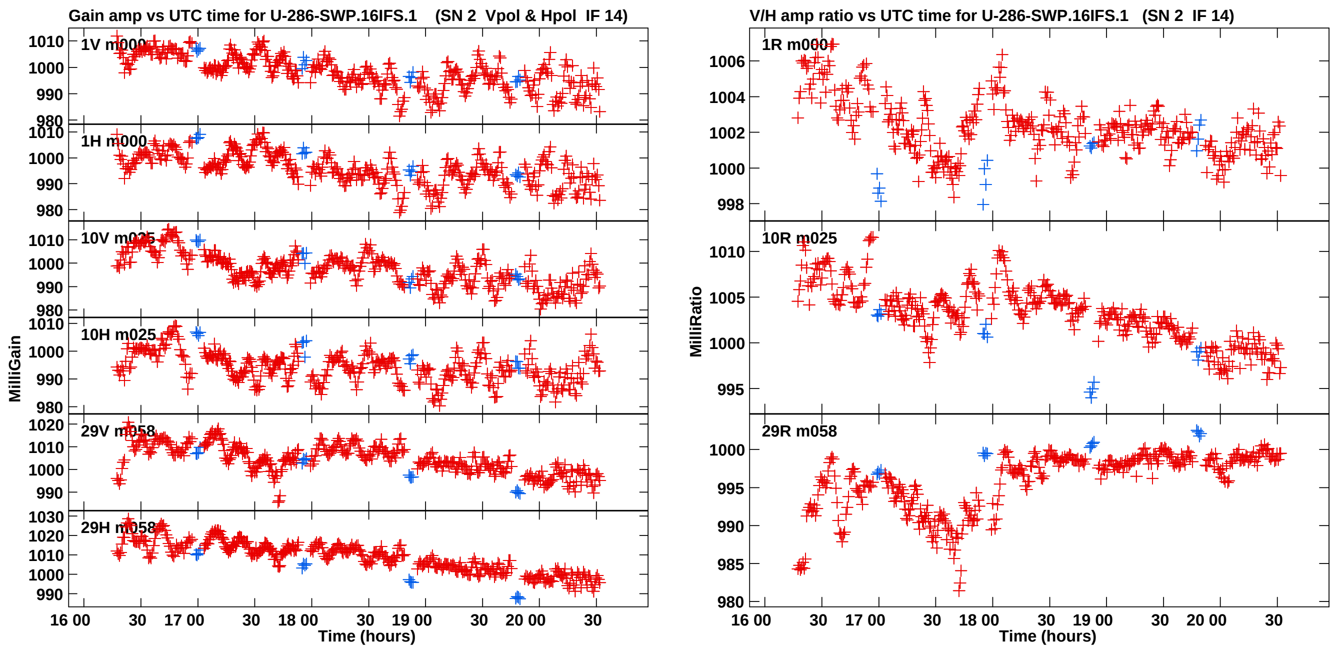

Figure 5: Amplitude gain solutions from J1939-6342 (blue) and J1331+3030 = 3C286 (red). The left panel shows the V and H gains for three representative antennas, the right panel shows the ratio of the amplitude gains.

is shown in the right panel. We note again the overall excellent stability of the MeerKAT gains. The $\sim 1\%$ gain fluctuations seen in the 3C286 solutions are due to the effects of background sources visible within the primary beam. It is easily seen that these fluctuations are common to both polarizations. The ratio of these gains is shown in the right panel – the typical deviations in the voltage gain ratios are typically less than $\sim 0.5\%$.

Note that the difference in gain solutions between 3C286 (red) and J1934-6342 (blue) are very small – less than 1%, despite an angular separation of over 100 degrees. Calibration using the latter source alone would have been sufficient to establish the amplitude gains to better than 1%, sufficient for most ordinary imaging projects.

The importance of accounting for calibrator source polarization in the generation of the parallel-hand gains is shown in Fig 6. Here are shown the gain solutions from the highly polarized calibrator 3C286 when the source polarization is accounted for, and not. The green and blue traces give the estimated gains when the polarization properties of 3C286 are ignored. The orange and red traces show the gains when a simple (point-source) representation of the source polarization is included in the estimation. Even this simple level of approximation (for the I, Q, and U emissions are extended and not identical, so utiliziation of models of each is the correct procedure) is sufficient for gain accuracies to better than 1%.

An important point of emphasis is that *if* the V and H gain *ratios* are sufficiently constant, then it may be possible to ignore the calibrator source polarization in the gain determination, provided that the resulting solutions in 'V' and 'H' are averaged before application. This works because the effects of the source linear polarization are opposite in the VV and HH correlations – see equations 4 and 7. If this approach is taken, it is important to ensure that any V/H amplitude gain ratio be removed before the gain solutions are made– in our case, this was done by the use of 'absolute' bandpass calibration from the unpolarized source J1934-6342.

The issue of adequate polarization models for calibrators is more complicated than it may seem. A calibrator's polarization structure can be quite different than that of Stokes 'I', and will commonly have a strong rate of change with frequency, due to source Faraday rotation. If the source RM (rotation measure) is high enough, Q and U can change sign within a subband, making traditional calibration methods inoperative. In such a case, a method related to 'Rotation Measure Synthesis' will be required.

The question of the necessary V and H stability to enable use of a polarized calibrator with unknown polarization will be answered by the required fidelity in the imaging. A discussion of this important point lies beyond the scope

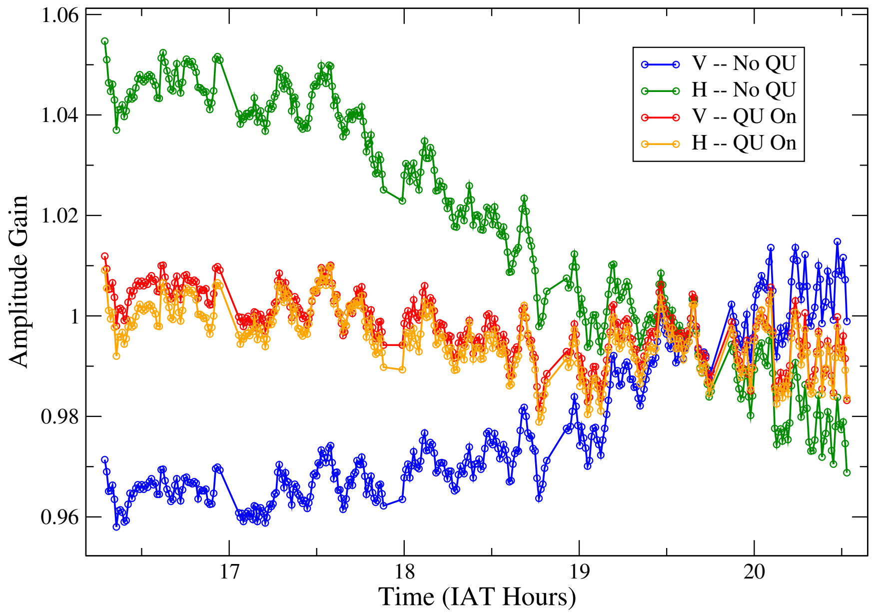

Figure 6: The effect of not accounting for the polarization state of the calibrator 3C286. The green and blue traces show the resulting gain estimates when the source polarization is ignored. The red and orange traces show the gains when the polarization properties are included.

of this memo. For the images shown later in this memo, the intrinsic stability of the MeerKAT electronics was sufficient.

Extremely high dynamic range imaging will certainly require independent solutions for each polarization, which will in turn require detailed models in Stokes' I, Q, and U (and in extreme cases, V), combined with, at low frequencies, a reasonable knowledge of the target source rotation measure.

4.6 Leakage and Feed Orientation Calibration

The term 'leakage' refers to signals from one polarization channel 'leaking' into the other. There are two mechanisms which cause leakage in our model:

1. The feeds are misaligned by angle θ. In this case, the voltage arising from the true vertical component of the incoming electric field will appear in both feeds – reduced by a factor $\cos\theta$ in the (nominal) feed, while a voltage proportional to $\sin\theta$ is introduced into the nominally orthogonal feed. This effect is parameterized by the misalignment angle θ. For the simple model we are using, the two feeds are coplanar, so there is no phase offset, hence the misorientation appears solely in the real part of the 'D' term.

2. Couplings within the electronics or due to antenna geometry will 'mix' the signals, transfering some of the 'vertical' signal into the 'horizonal' channel, and vice versa. These combinations are independent of the feed orientations, and are quantified by the antenna polarization ellipticity, χ. This leakage can have arbitrary phase, so shows up in both real and imaginary parts of the 'D' term.

The optimum way to determine the 'leakage' terms is to make use of the full equation set, equations 16 through 19. However, AIPS does not have at present the ability to do this, so we utilize instead the equations appropriate for an unpolarized source with small leakage – equations 33 and 34– which employ the cross-hand correlations alone. Because the 'D' terms in these expressions are differences of two complex values, it is not possible to determine them absolutely – the usual procedure is to assume they are zero for one antenna-polarization – 'V' in our case. The resulting solutions are then relative to the reference antenna-polarization value. Thus, the derived feed rotation offsets will be relative to that of the reference antenna 'V' feed orientation, and the derived antenna ellipticities are relative to that of the reference antenna 'V' ellipticity. The errors in using this simplification are proportional to $|D|^2$, which are quite negligible for these nearly-pure linear systems.

The AIPS task 'PCAL' is employed for this task. As noted above, this must, at present, be run using an unpolarized source – J1939-6342 in our case. Antenna m002 was again chosen as reference. Typical output from this operation is shown in Fig 7. The figure shows the imaginary and real parts of the 'D' factors for antennas m000,

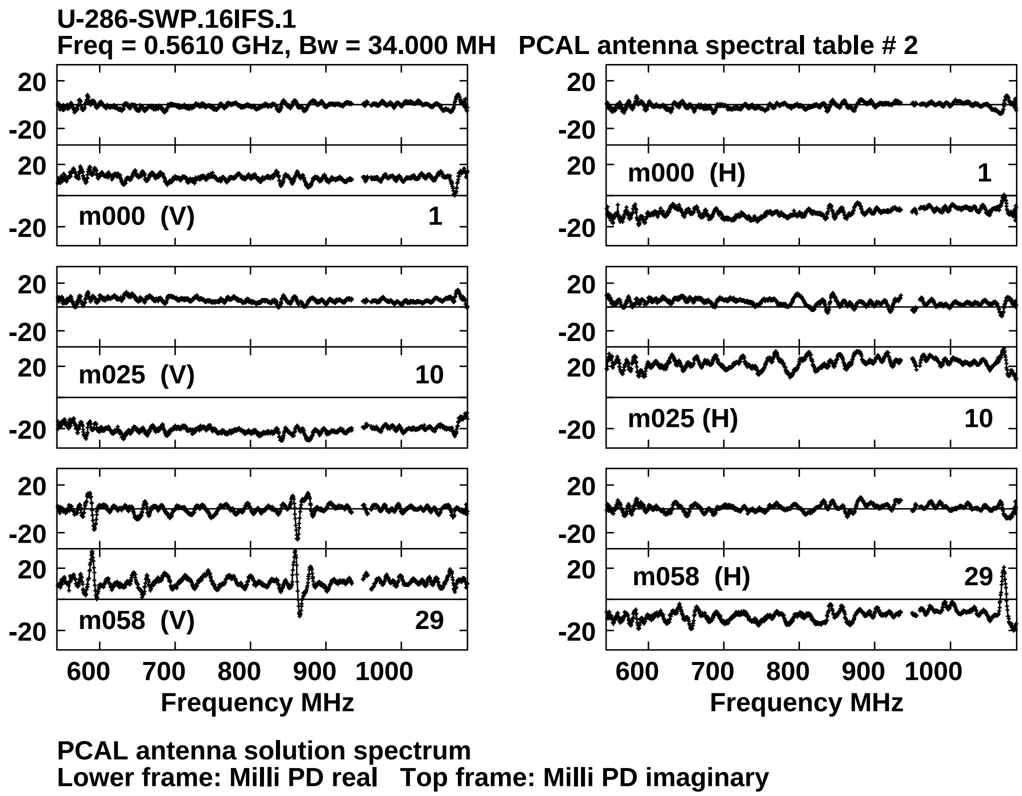

Figure 7: Showing typical cross-polarizations for the MeerKAT antennas at UHF band. Antenna m002 is taken as reference, meaning the polarization of its 'V' channel is assumed to be pure – zero orientation offset, and zero ellipticity. All values shown here are relative to these. For each of the six panels, the imaginary part (polarization ellipticity) is shown on top, the real part (feed orientation) is shown below. 'V' polarizations on the left, 'H' on the right. Note that the imaginary parts are very small, indicating the polarization purity of the antennas is very good, while the real parts are much larger, and generally constant across the band, as expected for feed misorientation.

m025, and m058. The 'V' polarizations are on the left, the 'H' on the right. Each panel shows the imaginary part (ellipticity) above, and the real part (feed orientation) below for the antenna and polarization listed. All values are relative to the 'V' polarization of the reference antenna, m002. The units are in milli-radians, so for the ellipticity, the ratio of the minor to major axes is typically 0.5%. The misorientations (w.r.t. the m002 'V' channel) are typically less than one degree, although for some antennas, it is as large as 3 degrees. Note that the real parts are nearly constant across the entire band – a result of the primary origin being the feed orientation. Note also that the sign of the real part is always reversed between the 'V' and 'H' solutions – this is a manifestation of the negation seen in equation 34 – negation meaning rotation by 180 degrees in the complex plane. Finally, the signs of the real part signifies the direction of misrotation (w.r.t. the reference) – a positive real part of the 'V' leakage indicates a positive (CCW) rotation of the feed, a negative real part indicates a negative (CW) rotation.

The imaginary parts of 'D' shown in Figure 7 are extremely small – always less than 0.01 for all antennas, indicating that the antenna polarization ellipses are nearly perfectly linear.

4.7 Cross-Hand Phase Calibration

We now return to the issue of cross-hand phase. The discussion in Section 3 ignored this factor, other than showing the effect of a negated sign (phase shift of 180 degrees) applied to one feed signal. In fact, the different electronic signal paths for the two polarization channels, and the residual cross-hand delays, will in general cause a differential phase of arbitrary value between them – quite separate from any possible 'wiring errors' of the dipoles.

The calibration procedures involving the delay, bandpass, and gain determinations operate independently for the two parallel-hand polarization channels. In fact, there will be a phase difference between the two channels, which will in general be frequency-dependent.

Examples of the phase differences between parallel-hand channels – w.r.t. the reference antenna – are seen in the right-hand panel of Fig. 3. This shows V-H phases of approximately 50, 65, and -74 degrees for antennas m000, m025, and m058, respectively. The 32 antennas utilized for the UHF band observations of 3C286 display a very wide range of V-H phases – essentially a uniform distribution from 0 to 360 degrees: eight antennas within 45 degrees of the reference, 12 antennas between 45 and 90 degrees, 3 antennas between 90 and 135, and 8 antennas between 135 and 180 degrees of the reference. These differences are removed by parallel-hand calibration, after which all cross-hand correlations share the same phase – that of the reference antenna, which must be determined by other means.

The best way to measure and remove this residual cross-hand phase would be an injected noise calibration system, installed on at least one antenna (the reference), which continuously monitors the frequency-dependent differential phases between the two polarization channels. MeerKAT has this capability which is deployed as part of the initial delay calibration. However, there is a residual delay left after this calibration, due to components situated 'upstream' from the injected calibration signal. This leads to small (up to 100ps) residual delays, which must be removed via astronomical calibration.

The procedure for finding and removing the V-H phase difference of the reference antenna is derived from a simple analysis of the observational effect of the phase offset between the parallel-hand channels for observations of a polarized source. Let us assume that the cross-polarizations ('D'-terms) are negligible, and that the parallel hand calibration has been applied. Then, the only remaining factor of concern is the cross hand phase difference of the reference antenna, denoted here by ϕ, defined as the phase offset of the 'H' channel with respect to the 'V' channel.

Including this phase offset, the responses for the cross-hand correlations can then be written (from eqn 5 and 6):

$$2R'_{v1h2} = e^{-i\phi}[-\mathcal{Q}\sin(2\Psi_p) + \mathcal{U}\cos(2\Psi_p) + i\mathcal{V}] \tag{44}$$
$$2R'_{h1v2} = e^{i\phi}[-\mathcal{Q}\sin(2\Psi_p) + \mathcal{U}\cos(2\Psi_p) - i\mathcal{V}] \tag{45}$$

where the 'prime' means the parallel-hand calibration has been applied. Note that these equations are in the antenna frame – *i.e.* they have not been corrected for the rotation caused by the parallactic angle. The parallel-hand responses are unaffected by the crossed-hand phase offset, so retain the forms given in equations 24 and 27.

If the Stokes visibilities are then generated without applying the rotation to offset the known parallactic angle, the values derived $\mathcal{I}'$, $\mathcal{Q}'$, $\mathcal{U}'$, $\mathcal{V}'$ are related to the true ones $\mathcal{I}$, $\mathcal{Q}$, $\mathcal{U}$, $\mathcal{V}$ by (using equations 9 through 11 with $\Psi_p = 0$ and equations 4, 7, 44 and 45,)

$$\mathcal{I}' = \mathcal{I} \tag{46}$$
$$\mathcal{Q}' = \mathcal{Q}\cos 2\Psi_p + \mathcal{U}\sin 2\Psi_p \tag{47}$$
$$\mathcal{U}' = (-\mathcal{Q}\sin 2\Psi_p + \mathcal{U}\cos 2\Psi_p)\cos\phi + \mathcal{V}\sin\phi \tag{48}$$
$$\mathcal{V}' = (\mathcal{Q}\sin 2\Psi_p - \mathcal{U}\cos 2\Psi_p)\sin\phi + \mathcal{V}\cos\phi \tag{49}$$

Note that the effect of a cross-hand phase offset is to rotate the linearly polarized visibilities $\mathcal{Q}$ and $\mathcal{U}$ into Stokes' $\mathcal{V}$, and vice-versa, with the amount depending on the parallactic angle and cross-hand phase. For an equatorial antenna, $\Psi_p = 0$ or 180, making the interchange be between $\mathcal{U}$ and $\mathcal{V}$ only[17]. For an alt-az antenna, the mixing depends on the parallactic angle, so changes over time, which has a very useful application, as discussed below[18].

Equations 44 and 45 then offer us a convenient way to solve for ϕ, provided the source has *either* no circularly polarized emission ($\mathcal{V} = 0$), *or* no linearly polarized emission ($\mathcal{Q} = \mathcal{U} = 0$). The former case is of interest here, for which the V-H phase becomes, from equations 48 and 49:

$$\tan\phi = -\mathcal{V}'/\mathcal{U}' \tag{50}$$

Note that this expression is independent of the parallactic angle, and does not require knowledge of the polarized flux. It is, however, necessary there be enough polarized signal so the value of $\mathcal{Q}\sin 2\Psi_p - \mathcal{U}\cos 2\Psi_p$ be measured with sufficient SNR. If the calibration observation is taken at a parallactic angle $\Psi_p = \Psi_{src}$, then $\mathcal{U}' = \mathcal{V}' = 0$, and the ratio becomes indeterminate. This also occurs when $\Psi_P - \Psi_{src}$ ± 90, or 180 degrees. Fortunately, since the

[17] Note also that if the cross-hand phase is 180 degrees, then the signs of U and V are negated, as shown in Section 3.

[18] For a more complete discussion of the effects of crossed-hand phase on polarimetric imaging, for both linear and circular systems, see EVLA Memo#207.

parallactic angle of a source changes with time, this 'null' problem can be avoided if observations are taken over a sufficient range in Ψ_p.

However, an ambiguity remains – equation 50 provides the same solution if the signs of both $\mathcal{U}'$ and $\mathcal{V}'$ are negated – i.e., we cannot tell if the solution is ϕ, or $\pi - \phi$. This is the cost of not utilizing the known values of the polarized signal. The solution to this is to utilize prior knowledge of the true value of $\mathcal{U}$, which brings us to investigating the cross-hand data of the polarized source 3C286.

As noted earlier, the linear polarization of 3C286 is well known, so we know the expected cross-correlation visibilities, VH and HV. Shown in Fig 8 are these expected visibilities, and the observed cross-hand data for one of the UHF 'spectral windows' for 3C286. Basic calibration for the delays and parallel-hand gains has been applied, as described in the preceding sections. The expected phases are zero for parallactic angles less than 205 degrees, since

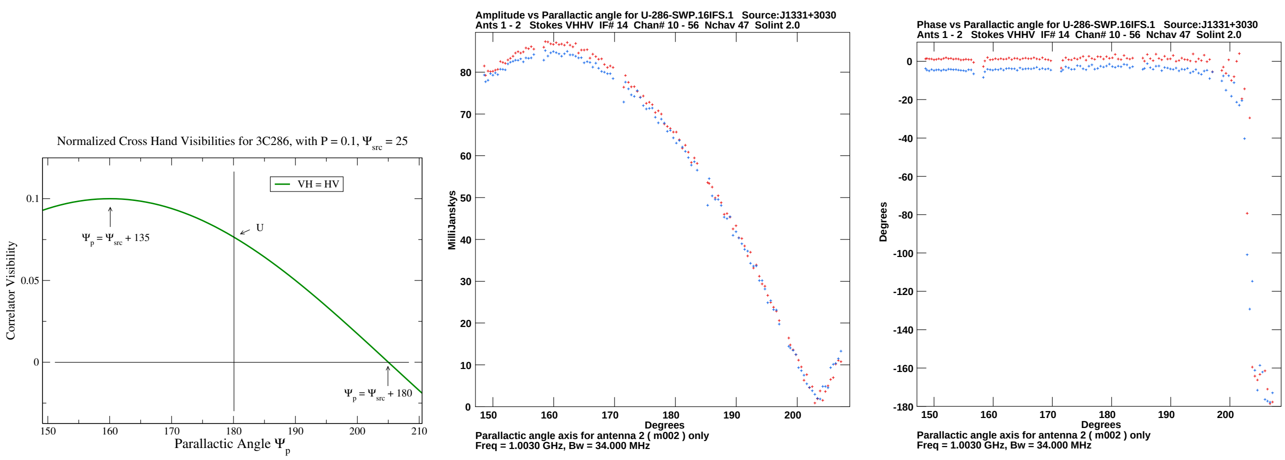

Figure 8: **Left Panel** Showing the predicted normalized crossed-hand visibilities for 3C286 at 1.00 GHz taken with MeerKAT. **Center Panel** The observed cross-hand visibility amplitudes on 3C286. Note that the 'rebound' on the right side of this panel reflects negation of the phase.**Right Panel** The corresponding cross-hand visibility phases. These indicate that the true cross-hand phase is near zero, so that the reference antenna feed V-H phasing is close to correct. The small difference in phases between the VH and HV traces indicates either a small value of $\mathcal{V}$, or a small V-H phase offset.

the visibility amplitudes shown in the left panel are positive. The observed phases, shown in the right panel, show a small deviation from zero, with opposite signs for the two correlations. The difference is twice the cross-hand phase (presuming V = 0). .

In AIPS, the solution for the cross-hand phase is provided by the task 'VHDIF', which forms the $\mathcal{V}'$ and $\mathcal{U}'$ visibilities *in the antenna frame*, then solves for the phase from their ratio. Because of the ambiguity noted above, the program offers two paths – one for the case where $|\phi| < 90$ (DOINVERS = 0), and the other when $|\phi| > 90$ (DOVINVERS = 1). Which to use can be determined by first plotting the phase of the cross-hand correlations for the known calibrator. Somewhat cruder, but probably simplest, is to try 'DOINVERS = 0', then plot the visibility phases for the Q and U Stokes for the polarized calibrator. They must be either zero or 180, depending on the EPA of the calibrator source. If these are not as expected (for 3C286, both must be zero, since Q and U are both positive), then re-run VHDIF, with 'DOINVERS = 1'.

Alternatively, the correct solution could be derived directly from examination of equations 44 and 45 separately, but this would require knowledge of the calibrator source polarizations. The advantage of the method chosen in AIPS is that it is independent of the value of the linear polarization.

We noted earlier that no solution will be possible when $\mathcal{U}' = \mathcal{V}' = 0$, and that this condition will occur when the parallactic angle equals the source polarization position angle or that angle plus 90, 180, or 270 degrees. This problem will be avoided by ensuring multiple (at least two) observations of a strongly polarized source at significantly different parallactic angles through the run. The VHDIF program allows a single solution, formed by combining all cross-hand data from the highly polarized calibrator, or multiple solutions over time, each derived from a short segment of data. This option is useful for checking if there is a temporal drift in the cross-hand delays or phase[19]. The effectiveness of utilizing multiple solutions is shown in Fig 9, showing cross-hand phase solutions.

[19]We found no significant temporal changes in the MeerKAT data.

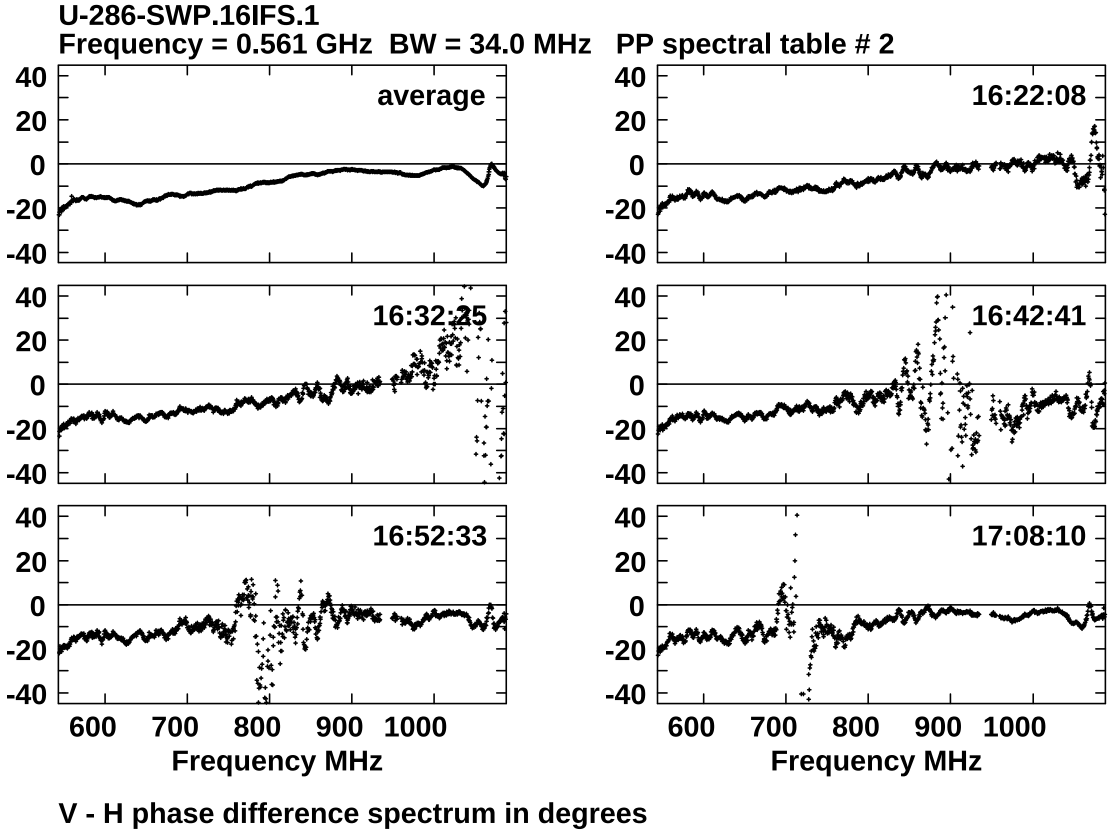

Figure 9: Showing the cross-hand phase solutions. The upper left panel shows the solution obtained by averaging over all the data taken over a four-hour span. The remaining panels show individual solutions derived from 10-minute integrations. The noisy solutions moving from right to left in these panels (from high frequency to low) reflects the $\mathcal{U}' = 0$ condition, combined with the steady rotation of the source's polarization position angle over frequency.

Shown in the figure are the averaged solution in the upper left panel, and five separate solutions, each generated from a 10-minute integration. The visible slope in the average phase solution represents a small cross-hand delay[20] of about 100ps. Phase fluctuatations about this mean slope are no more than 10 degrees. The individual solutions nicely illustrate the problem when $\mathcal{U}$' goes to zero, which results in no significant signal from which to estimate the phase offset. For a source with zero RM, the condition will apply to all frequencies at the same time – hence our recommendation that at least two observations be made. For 3C286 in our example, the EVPA is a strong function of frequency, so the $\mathcal{U}' = 0$ condition will be met at different times (= different parallactic angles) for different frequencies. This is seen in the figure by the movement of the poor SNR solutions from higher to lower frequencies as the time progresses.

The value of the cross-hand phase affects the phase of the 'H' polarization in the BP table, and the phases in the PD table. VHDIF will update these tables after it finds the average cross-hand phase.

Unfortunately, the issue of which antenna to choose for the reference is not straighforward. All phases are relative in interferometry, so there must be in general a reference antenna. In the UHF band, for example, the distribution of the 'V-H' phase differences amongst the antennas is nearly uniform from 0 to 360 degrees (three examples are shown in the right panel of Figure 3). With the current calibration method used in AIPS for the determination of the cross-hand phase, the selection of the DOINVERS adverb in VHDIF is entirely dependent on the choice of reference antenna. Selecting the correct value requires examination of the cross-hand visibility phases, or of the derived Q and U values after calibration. Automating this process is not (yet) implemented in the procedure. At this time, the simplest, and safest, procedure is to use the value of DOINVERS which produces the correct value of the polarization calibrator Q and U.

[20]This residual delay could be removed by a cross-hand delay solution, which we opted not to try.

5 MeerKAT Characteristics at L and S bands

The examples shown in preceding sections are taken from analysis of the UHF data. Here we show examples of the gain, bandpass, and polarization solutions for the data taken at L and S bands.

The parallel-hand phase solutions, and V-H phase differences at L- and S-bands are shown in Fig 10. L-band solutions are on the left side, S-band solutions on the right. Both bands show excellent phase stability overall.

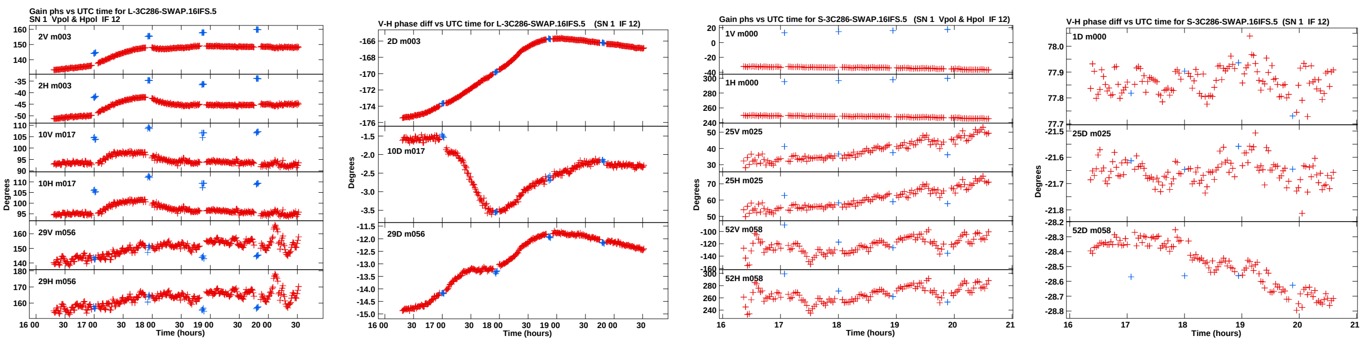

Figure 10: The phase, and phase differences for three representative antennas at L-band (left) and S-band (right). The phase difference stability at L-band is much worse than that seen at both UHF and S-bands. The antennas chosen for the S-band display are the same as those shown for UHF band, in Fig. 3. The same phase offsets are seen.

However, the L-band V-H differential phase stability is much worse than UHF or S-bands, showing distinct trends which are different for each antenna. The S-band differential phase stability (right-most panels) is very good, and similar to that seen at UHF band. The origin of the L-band drifts is not known to us. The effect is not large enough to severely affect the polarimetry.

The distribution of the V-H phase differences amongst the antennas is rather different amongst the three bands. At the UHF band, as noted earlier, the distribution is nearly uniform from 0 to 360 degrees. At L-band, the distribution is much narrower, 29 of the 32 antennas in the observation have differentials within 100 degrees of that of the reference. And at S-band, the distribution is still narrower, with nearly all of the 56 antennas within 80 degrees of the reference antenna.

Typical bandpasses are shown in Fig 11, with L-band on the left, and S-band on the right. The gaps in the L-

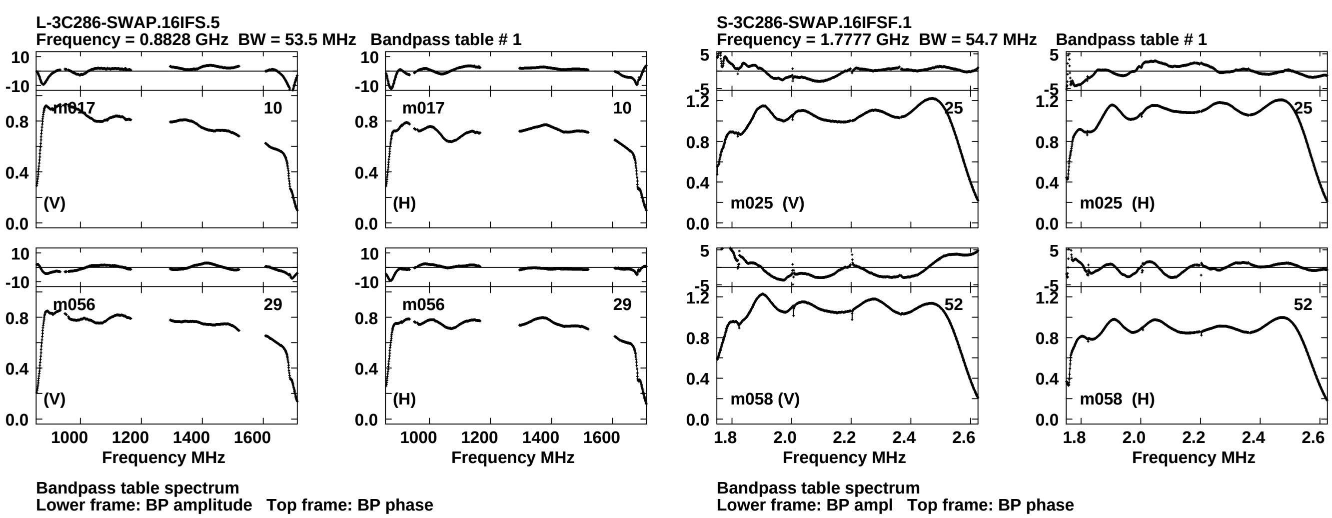

Figure 11: Typical bandpasses for four antennas at L-band (left) and S-band (right).

band bandpasses are due to strong RFI. In general, the S-band bandpass amplitude and phases show larger frequency undulations, with a typical period of 100 MHz. If due to reflections within the electronics, this corresponds to a distance of $\sim 1.5/\eta$ meters, where η is the cable index of refraction.

Typical amplitude gains and gain ratios are shown in Fig 12. Again, the L-band plots are on the left, the S-band plots on the right. Note that the $\sim$1% gain fluctuations seen in the UHF band gains are much reduced at these

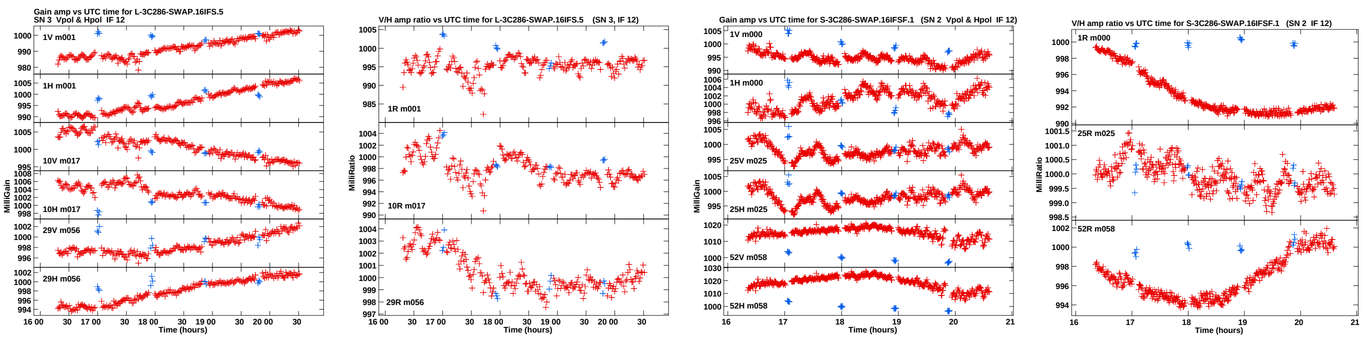

Figure 12: The amplitude, and amplitude ratios for three representative antennas at L-band (left) and S-band (right).

higher frequencies, a result of the reduced confusion from background sources. On the other hand, the S-band gain ratios show clear temporal trends, which are different for different antennas. For the two antennas shown which have these trends (m000, and m058), the observed variations are in 3C286 only, suggesting an origin related to the low elevation of 3C286. Note that it is the 'H' channel gains that appear responsible for these observed variations in the ratios.

Typical cross-polarization solutions are shown in Fig 13, again with L-band on the left, and S-band on the right. The values of the real parts (orientation offsets) in the S-band solutions are much larger in many antennas than those

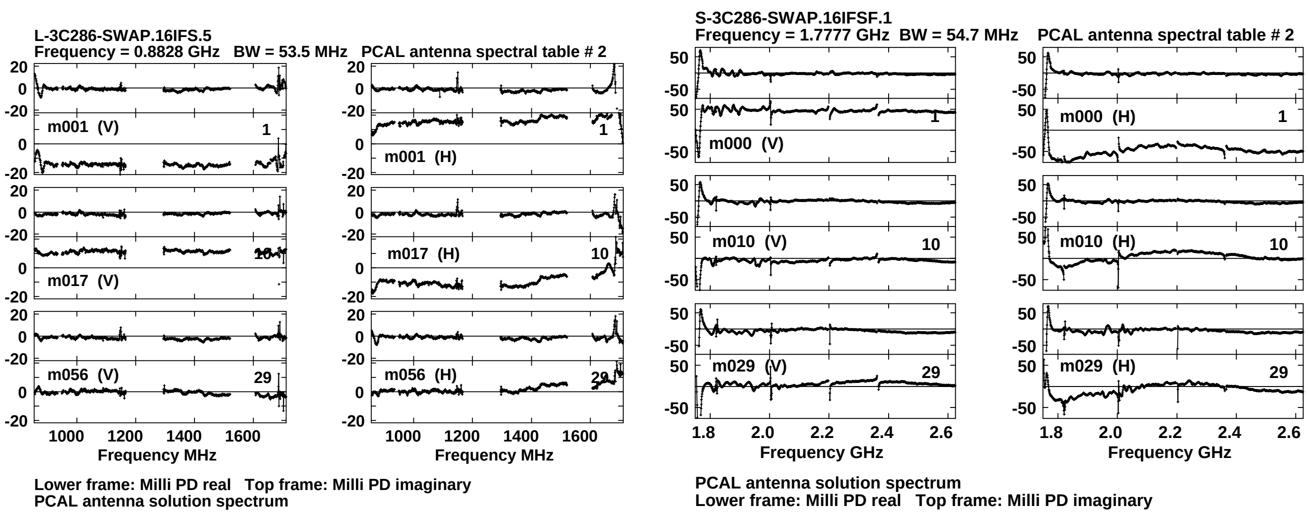

Figure 13: Cross-Polarizations at L-band (left) and S-band (right). The H channel orientation parameter (real part) for S-band (right panel) is considerably larger than at the other bands, and shows a distinct curvature over frequency. This curvature suggests an origin other than feed orientation.

seen at the other bands. Some exceed 3 degrees. Furthermore, striking frequency curvatures are visible in the 'H' real parts, with different amplitudes, but the same frequency period, in most of the antennas (including the three shown in the figure). The straightforward interpretation of different feed orientations at different frequencies is not viable here, so the origin must be signal coupling between the channels occuring in the electronics.

The cross-hand phases for the reference antennas at L and S bands are shown in Fig 14, with L-band again on the left, and S-band on the right. Note that for the S-band cross-phase, the values are near 180 degrees, indicating the need to negate the sign of the 'H' channel in order to obtain the correct sign of Stokes 'U' in 3C286 – the horizontal dipole is, in effect, reverse-wired w.r.t. the vertical dipole. We found this to be the case for all S-band antennas, so the origin is due to receiver construction. The overall slopes in these two plots are due to residual delay between the two polarizations in the reference antennas: about 80 ps at L-band, and 25 ps at S-band.

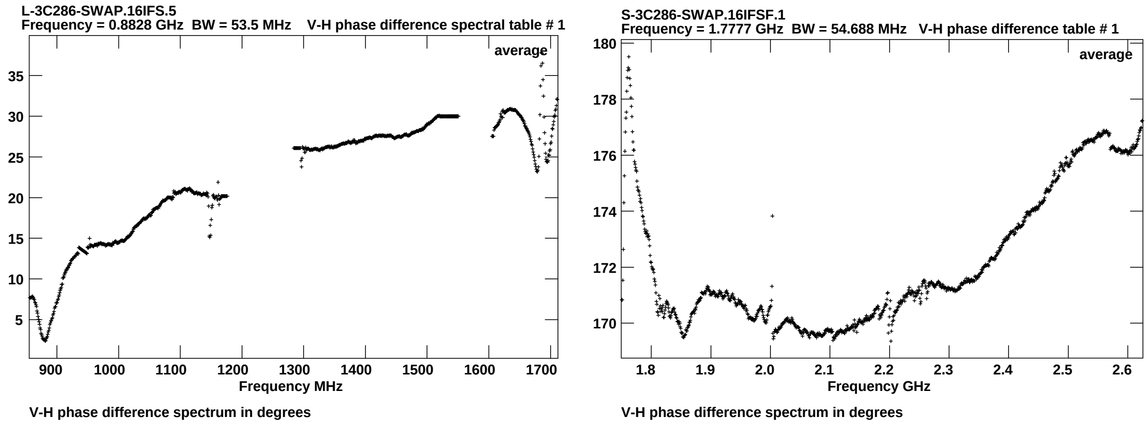

Figure 14: The cross-hand phase (of the reference antennas) for L and S bands. The S-band values are near 180 degrees, indicating the 'wiring' of one dipole is reversed, with respect to the standard.

6 Some Nice Results

Following the calibrations described above, full-field images of 3C286 were generated in I, Q, and U and V for one of the 'spectral windows' in each band. The dynamic range in all of them is very good – typically 10,000 – 20,000:1 in 'I', and 5,000 – 10,000:1 in polarization. This is especially impressive, given that no 'calibration/imaging tricks' were utlized in the calibration – the calibration utilized a single point-source model, so the effects of the background sources, and all 2nd-order effects in the polarization calibration were ignored.

Is is difficult to effectively display these full-field maps, so we show in Fig 15 three contour plots of a small polarized background source, located about nine arcminutes to the NW of 3C286. These images have been primary-

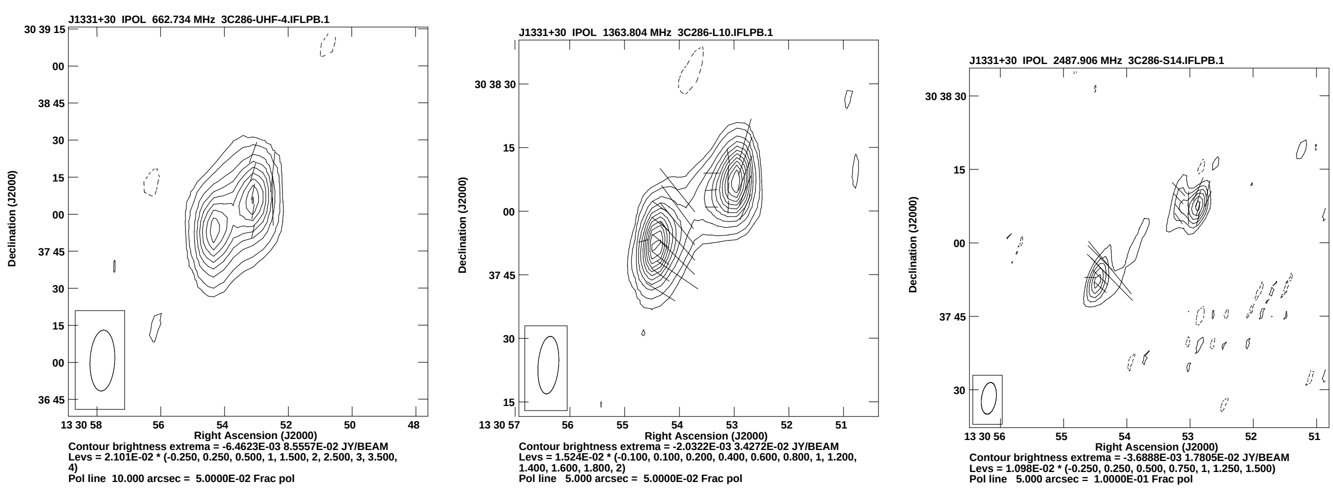

Figure 15: Contour plots of a small double radio source, located 9 arcminutes to the NW of 3C286. These are a small window from a full primary beam image. All have been corrected for primary beam attenuation, but not for beam-induced polarization. **Left Panel** UHF Band at 667 MHz. Resolution 10 by 25 arcsecond. Full image peak: 21 Jy/beam. Image rms 1.6 mJy/beam.**Center Panel** L-band at 1360 MHz. Resolution 4.9 x 13.6 arcseconds. Full image peak: 15.2 Jy/beam. Image rms: 0.5 mJy/beam. **Right Panel** S0-Band: 2490 MHz. Resolution 6.5 x 3.0 arcseconds. Full image peak: 11.0 Jy/beam. Image rms: 1.6 mJy/beam.

beam corrected, but have not been adjusted for any beam polarization signature.

We also generated I, Q, and U images of 3C286 for each 'spectral window' (defined by our use of MORIF, which broke the spectral span into 16 adjacent windows) for each band. The resulting polarization properties of 3C286 are shown in Fig 16.

The two left panels show the fractional polarization (top) and EVPA for 3C286, as a function of frequency. The colored lines indicate the observing band – black for UHF, red for L, and blue for S bands. The right side panels

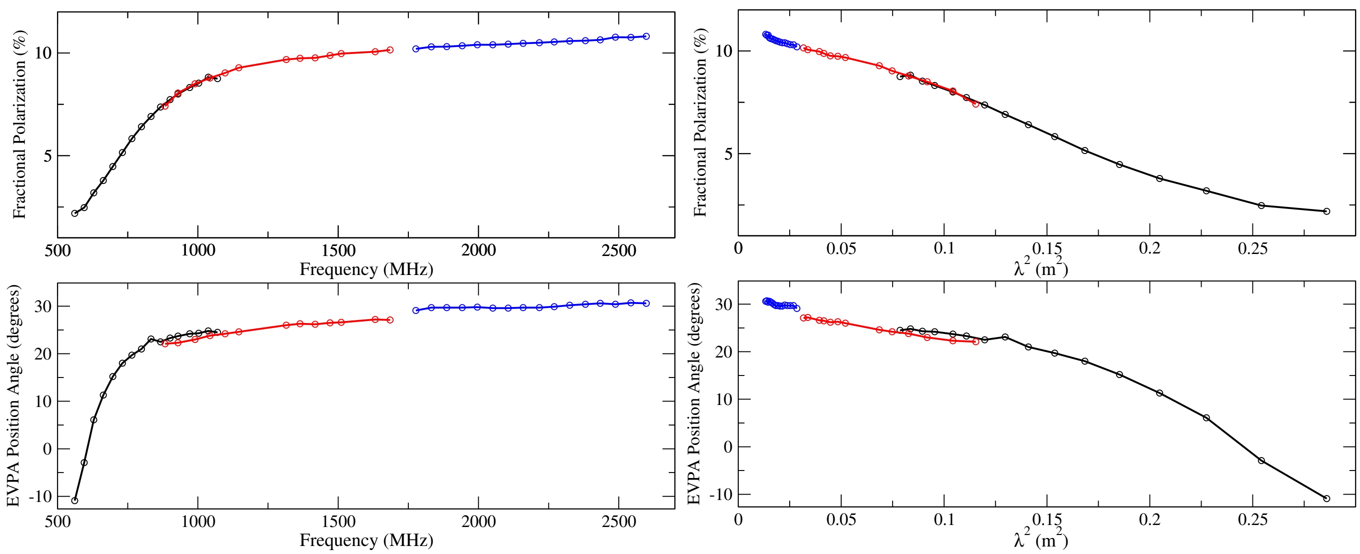

Figure 16: The observed polarization properties of 3C286, using the MeerKAT data. The UHF, L and S band data are shown in black, red, and blue, respectively. These are provisional results, which have not been corrected for ionospheric rotation, or offsets due to the reference antenna feeds. **Left Panel** The fractional polarization (top) and EVPA position angles(bottom) as a function of frequency. **Right Panel** The same, as a function of λ^2. The data, down to a frequency of about 800 MHz, can be fitted with rotation screen with RM $\sim$ -1.5 rad/m/m.

show the same data, as a function of λ^2. The smooth decline in the fractional polarization with decreasing frequency is commonly observed in most compact radio sources. The values shown here are in excellent agreement with those determined (above 1 GHz) by the VLA. The small difference in EPA seen at L-band (red points in the lower figures) is likely due to a slightly misaligned feed in the reference antenna utilized in the calibration.

The bottom right plot suggests two different Faraday screens are in operation – one with RM~ -1.5 rad/m/m seen at higher frequencies, and a much thicker screen, at lower frequencies. However, the steady decline in fractional polarization strongly implies the situation is more complicated than two screens covering different regions of the source. More likely is a complicated magnetized screen, combined with spectral index variations across the source emission.

The EPA values shown have not been corrected for any rotations due to the ionosphere, or the offset in orientation of the feeds on the reference antenna. Hence, the values shown are not to be construed to be a new model for the polarization properties of 3C286. This will be the subject of an upcoming memo which will include data from both MeerKAT and the VLA.

7 Summary of AIPS Processing

Listed here are the sequence of tasks utilized to calibrate the data. It is assumed that data are provided as a FITS-format file.

- FITLD, to load the data into AIPS. The polarization assignments are automatically adjusted.
- MORIF, to divide the continuous MeerKAT bandpass into 16 adjacent 'spectral windows'.
- UVFLG, CLIP, etc., needed to remove RFI and other corrupted data.
- FRING and CLCAL to determine and apply parallel-hand delays and phases. (SN1 and CL2)
- BPASS to determine the bandpass functions, using an unpolarized source. (BP1)
- CALIB and CLCAL to determine and apply the parallel-hand gains. If a polarized calibrator is utilized, the polarization state must be known in advance if the 'V' and 'H' solutions are to be applied separately. (SN2 and CL3)
- PCAL to determine the cross-hand leakages. At this time, the source must be unpolarized. (PD1)

- VHDIF to find and remove cross-hand phase and delay. Due to an ambiguity, two executions may be needed, with and without a 180 degree phase inserted. (PP1, PD2, BP2)
- UVPLT of the cross-hand phases for the polarized calibrator (or IMAGR to generate Q and U images). If these are not correct, rerun VHDIF with the opposite sign for the cross-hands.

8 Summary

AIPS is now able to calibrate and image interferometric data taken with linearly-polarized antennas. Observations taken with MeerKAT have shown excellent results, with image dynamic ranges, in all Stokes' parameters, of many thousands to one – easily equal to the performance of the VLA. It is hoped that the description given here will be of assistance to commissioning efforts for future arrays, in particularly the NGVLA.